SOLITARY-WAVE COLLISIONS

JOSEPH HAMMACK
Department of Mathematics, Penn State University
University Park PA 16802 USA

DIANE HENDERSON
Department of Mathematics, Penn State University
University Park PA 16802 USA

PHILIPPE GUYENNE
Department of Mathematics & Statistics, McMaster University
Hamilton, Ontario L8S 4K1 CANADA

MING YI
State College High School
State College PA 16801 USA

Dedication

This paper is dedicated to Professor Theodore Yao-Tsu Wu, a gentleman, a scholar, and my teacher. His lectures on "Hydrodynamics of Free Surface Flows" provided inspiration for my fascination with, and study of, water waves. His research provided the standard of rigor and precision to which I strive. I am honored and grateful that our lives intersected.

Joe Hammack

Experimental and theoretical results are presented for binary collisions between co-propagating and counter-propagating solitary waves. The experiments provide high-resolution measurements of water surface profiles at fixed times, thereby enabling direct comparisons with predictions by a variety of mathematical models. These models include the 2-soliton solution of the Korteweg-deVries equation, numerical solutions of the Euler equations, and linear superposition of KdV solitons.

1. Introduction

The study of solitary-wave collisions has an old and venerable history that dates from the seminal experiments reported by John Scott Russell in 1845. His discovery of the solitary wave precipitated many mathematical investigations that provided a theoretical foundation and physical understanding for many of its interesting properties. In particular, Korteweg & deVries (1895) derived their

now famous equation for water waves propagating in one direction on shallow water. Moreover, they found an exact solution of the KdV equation for a single wave that is localized in space and propagates without change of form-the solitary wave.

Both the deeper mathematical and physical significance of the solitary wave was not realized until the subsequent development of "soliton theories" that was initiated by Gardner, Greene, Kruskal & Miura (1967). GGKM demonstrated a method to solve the KdV equation exactly on the real line for a wide class of localized initial data. Their results showed that initial data evolve into a finite number of co-propagating solitary waves, rank ordered by their amplitude (largest first), and a trailing train of dispersively decaying waves. Each of these solitary waves is referred to as a "soliton" based on the previous work of Zabusky & Kruskal (1965) who coined the name for particle-like waves that collide "elastically", i.e., they emerge from a collision with no change in form. This collision property of solitary waves was made explicit by the exact, N-soliton solutions of the KdV equation found by Hirota (1971), who showed that the only lasting evidence of a co-propagating (following) collision is a phase shift in space. Weidman & Maxworthy (1978) provided much experimental collaboration of predictions based on Hirota's exact solution for two solitons, e.g., phase shifts. In particular, they used photography to obtain spatial data at fixed times. These photographs provided qualitative results (only) for spatial profiles in consequence of the disparate vertical and horizontal wave scales of solitary waves.

Studies of binary collisions of counter-propagating solitary waves appear to have been initiated analytically by Mayer (1962). Byatt-Smith (1971) derived an explicit, approximate prediction for the maximum runup amplitude for the head-on collision of two equal-amplitude solitary waves. This special case is often used to model the reflection of a solitary wave by a vertical wall, and much of the literature concerns this special collision case. Cooker, Weidman & Bale (1997) provide an excellent literature review as well as new numerical results for the special case of solitary-wave reflection by a vertical wall. (This special case is not the focus of the present study, and will not be reviewed here.) Maxworthy (1976) presented cinematic-based measurements of phase shifts and maximum runup amplitudes for two counter-propagating solitary waves. Maxworthy did not present detailed spatial profiles during the interaction, and the presented data showed considerable scatter. We note that, like the photographs of Weidman & Maxworthy (1978), the cinematic-based measurements did not resolve vertical wave structure with high resolution. Su & Mirie (1980) and Mirie & Su (1982) present approximate, analytical and numerical studies for the head-on collision of two solitary waves. They found that the collision was not elastic, i.e., in addition to small phase shifts a small amount of energy was lost by each of the waves to form secondary waves. This reduction in amplitudes leads to a reduction in wave speeds; hence, the phase shifts become spatially dependent.

Byatt-Smith (1989) obtained higher-order, approximate results for the head-on collision of solitary waves with unequal amplitudes, and confirmed the results of Mirie & Su (1982). Yih & Wu (1995) and Wu (1998) present analytical studies for head-on and following collisions of solitary waves of unequal amplitudes. In particular, Wu (1998) shows that there is an instant during both following and head-on collisions in which the spatial wave profile exhibits fore-and-aft symmetry.

Herein we investigate both the co-propagating (following) and counter-propagating (head-on) collisions of two solitary waves. Precise experimental data of spatial wave profiles at fixed times are presented and compared with the predictions of several mathematical models. For the head-on collision we use linear superposition of two KdV solitary waves and numerical solutions of the Euler equations. For the following collision we use the 2-soliton solution of the KdV equation and numerical solutions of the Euler equation. All of these mathematical models neglect viscous effects that are intrinsic in the experimental data. Obtaining high-resolution spatial measurements of experimental waves evolving in time and space is exceedingly difficult; hence, the emphasis of the discussions herein is on the experimental aspects of the study. The mathematical models are discussed briefly.

2. Experimental Program

In order to obtain quantitative experimental data for spatial wave profiles at fixed times that are needed for definitive comparisons with the mathematical models, it was necessary to develop special experimental facilities and procedures. The key idea is to use the most sophisticated electronic and mechanical systems available and to develop experimental procedures that enable us to repeat the same experiment over and over *as precisely as possible.* Indeed, the use of repeatable experiments to obtain spatial data at fixed times was the basis of Russell's pioneering work on the solitary wave. In order to understand both the strengths and limitations of the data that we obtained, it is necessary to provide a detailed accounting of this experimental program.

2.1 Wave Channel

Experiments were conducted at the W. G. Pritchard Fluid Mechanics Laboratory in a horizontal wave channel that was 13.165m long, 25.4cm wide, and 30.0cm deep. Channel walls and bottom were made of glass that was precisely aligned. Stainless steel rails spanned the channel along the top of the two sidewalls. These rails supported an instrumentation carriage whose motion along the channel was provided by a linear belt drive and motor. The carriage supported four wave gages, spaced 40cm apart, and their associated electronics. A 10m long section of the channel was used for the experiments. This section

was bounded by a vertical glass wall at its downstream end (x = 10m) and by a Teflon wave-maker piston at its upstream end (x = 0). A pressure gage was mounted at x = 7.155m in the center of, and flush with, the channel bottom.

2.2 Wave-maker

Solitary waves were generated by the horizontal, piston-like motion of a paddle made from a Teflon plate (0.5 inch thick) inserted in the channel cross-section. The paddle was machined to fit the channel precisely with a thin lip around its periphery that served as a wiper with the channel's glass perimeter. This wiper prevented any measurable leakage around the paddle during an experiment. Paddle motion was driven directly by a state-of-the-art *linear* motor and integral carriage with up to 55cm of stroke and a position resolution of 20,000 counts/cm. The motor and paddle assembly were supported over the wave channel by a separate steel frame.

2.3 Wave & Depth Measurements

In all experiments waves were measured by a bottom-mounted pressure transducer and by four, non-contacting, capacitance-type gages, 40cm apart, and supported above the water surface by the instrumentation carriage. The sensing element of the wave gages was about 6mm wide and extended 12.7cm across the channel, thereby providing an average cross-channel measurement of instantaneous water surface elevations. The sensing element was 3cm above the water surface, and this maximum-possible height limited the maximum wave amplitudes that could be used in the experiments. Each gage was supported on a rack-and-pinion assembly with motor so that it could be calibrated under computer control. The pressure transducer measured the bottom water pressure (head) in the range of 0-10.16cm with an output voltage in the range of 0-5V. Both the wave gages and pressure transducer have remarkably repeatable and linear calibrations.

Precise control of the quiescent water depth (h = 5cm) was essential during these experiments. Although a traditional point gage was used, we found that the pressure transducer provided much greater resolution and control. In fact, we were able to monitor the depth to within about 0.25mm, which corresponded to a water volume in the channel of one liter. This resolution enabled us to avoid significant depth changes during experimental series.

2.4 Data Acquisition & Control

Analog signals from the four wave gages and pressure transducer were low-pass filtered (30Hz) and digitized using a state-of-the-art (sigma delta technology) computer system that enables exactly simultaneous sampling among signal channels with 16-bit accuracy. The system runs under the (hard) real-time

operating system of VxWorks. Sampling was initiated by, and synchronized with, another real-time computer system (Programmable Multi-axis Controller by Delta Tau, Inc.) dedicated to control of the motors that generated the waves, calibrated the gages, and moved the instrumentation carriage. The integration of the data acquisition and control systems enabled an entire experiment to be performed under computer control.

2.5 Procedures

Since only four wave gages were available on the instrumentation carriage we could only measure waves at four spatial locations during a single experiment. To circumvent this limitation we exploited the technological sophistication of both the mechanical and electronic systems that enable the (near) repeatability of an experiment. First, an initial carriage position was chosen and an experiment conducted. Then the carriage was shifted 1cm downstream from its previous position and the experiment was repeated. Repeating this procedure 40 times provided a data set that spanned 1.6m in the x-direction (since the gages were spaced 40cm apart) with a resolution of 1cm. This data set could then be interrogated to provide spatial profiles of the water surface beneath the instrumentation carriage at any fixed time. Specific procedures differed for the head-on and following collision experiments, and are described below.

2.6 Wave Generation

The motion of the wave-maker was programmed to generate a solitary wave by forcing a (horizontal) velocity field in the water that is 'close' to that occurring during passage of a solitary wave. We adopted a procedure similar to that introduced by Goring & Raichlen (1980), which accounts in part for the finite displacement of the wave-maker paddle and the propagation of the wave during generation. Generation was based on the KdV solitary wave whose horizontal velocity field is given by:

$$u(x,t)=u_o \operatorname{sech}^2\left[\sqrt{\frac{3u_o}{4h_o^2 c_o}}\left(x-c_o t-\frac{1}{2}u_o t\right)\right] \qquad (1)$$

in which h_o is the quiescent water depth, $c_o=\sqrt{gh_o}$, g is gravitational acceleration, a_o is the wave amplitude, and $u_o=a_o c_o/h_o$ is the maximum horizontal velocity. The displacement x_p of the wave-maker paddle from its initial position (x=0) is then found numerically by solving the differential equation:

$$x_p'(t) = u(x_p, t), \tag{2}$$

which gives the Lagrangian path of a water particle. Figure 1 shows the resulting paddle motion (solid line) for a solitary wave used in both the head-on and following collision experiments with a_o = 2cm and h_o = 5cm. For convenience we also show (dashed line) the linear approximation of Equation

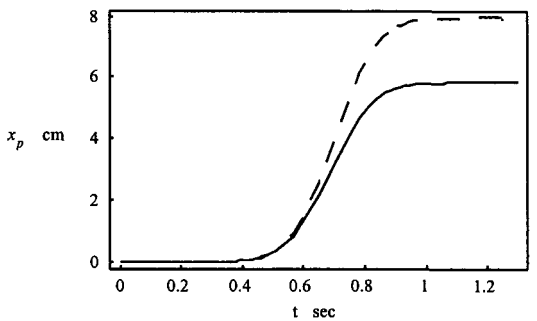

Figure 1. Wave-maker displacement for a_o=2cm. Solid line is solution of Equation (1). Dashed line is linear approximation.

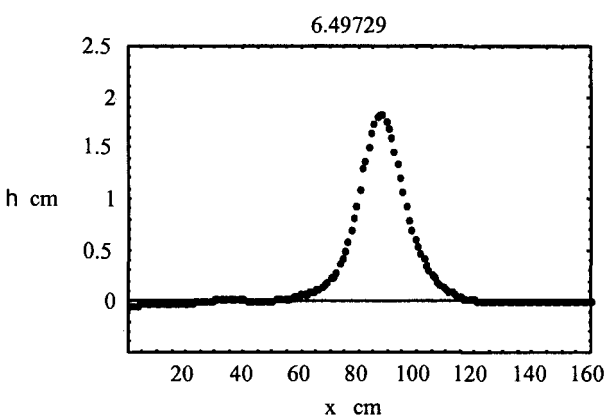

Figure 2. Experimental solitary wave generated with a_o = 2cm. Carriage window in the interval.

(1). An experimental measurement of the wave generated by the paddle motion of Figure 1 is shown in Figure 2. In this measurement the wave is propagating to the right underneath the carriage, which was positioned so that its 160cm measurement window was centered about x = 5m. The amplitude of the solitary wave is about 1.9cm in consequence of viscous damping during propagation from the wave-maker. Note that there is a small shelf–like wave, with a maximum amplitude of about 0.3mm, trailing the solitary wave, followed by even smaller, decaying, long-period oscillations that are barely perceptible.

2.6 Discussion

In spite of all efforts some small differences between two repeated experiments will occur. Three unavoidable sources of differences were recognized at the outset of the experimental program. The first of these sources is *latency*, which is inherent in all electro-mechanical servo systems. Latency is the small time interval between when an electro-mechanical system is commanded to move and when movement actually begins. A measure of this time is the servo update period, which is 0.885ms in these experiments.

A second source of experiment differences is water *surface contamination*. An exposed water surface accumulates surfactants with time (both from the air and fluid interior) that enhance wave damping during propagation. We conducted a series of experiments in which we measured damping of the solitary wave shown in Figure 2 at different times over a period of two days. We concluded that experiments would not be affected significantly by surfactant accumulation for up to six hours. After 6 hours, it was deemed necessary to drain and clean the channel and then refill it in order to begin the next series of experiments.

A third source of experimental differences is *residual boundary layer* motions that are left behind as a solitary wave propagates in the channel. In both the co- and counter-propagating binary collision experiments solitary waves encounter the boundary-layer wakes of the other wave. This wake does have a small effect on wave speeds that can be significant in our data analysis. Detailed measurements of these boundary layer motions were not made; hence, it is not known how reproducible they are.

It is straightforward to cope, in part, with the three sources of difference described above in our set of 40 repeated experiments. The pressure-gage measurements, which would be identical in exactly reproducible experiments, are used to time shift each experiment's measurement to yield the maximum correlation with the first experiment in the set. Typically, these time shifts were about 0.01s resulting in correlation coefficients greater than 0.99. The worst case we encountered required a time shift of about 0.06s and had a correlation coefficient of 0.964. This case produced significantly poorer results in the data analysis, and appears to result from an unanticipated and unavoidable random

fourth source of difference that occurs during the *reflection* of a solitary wave from a vertical wall. We discuss this phenomenon in more detail below.

3. Mathematical Models

We compare the experimental results with theoretical predictions of several initial-value mathematical models that assume incompressible, inviscid, and irrotational wave motions. Numerical solutions of the Euler equations are presented for both the head-on and following collisions. In addition we employ explicit analytical predictions based on the Korteweg-deVries equation(s).

3.1 Euler Model

Consider a two-dimensional layer of water in a domain defined by $\Omega(\eta) = \{(x,y) : x \in \Re, y \in [-h,\eta]\}$, in which $\eta(x,t)$ denotes the free surface elevation referenced to the quiescent water level $y = 0$, and $y = -h$ denotes a rigid bottom boundary. The velocity vector $\boldsymbol{u}(x,y,t)$ is given by $\boldsymbol{u} = \nabla\phi$ in which the velocity potential $\varphi(x,y,t)$ satisfies

$$\Delta\varphi = 0 \quad \text{in } \Omega(\eta). \tag{3}$$

On the bottom boundary, $y = -h$, the velocity potential satisfies the Neumann boundary condition:

$$\partial_y\varphi = 0. \tag{4}$$

The free surface boundary conditions on $y = \eta(x,t)$ are:

$$\begin{aligned} \partial_t\eta &= \partial_y\varphi - (\partial_x\eta)(\partial_x\varphi), \\ \partial_t\varphi &= -\tfrac{1}{2}|\nabla\varphi|^2 - g\eta. \end{aligned} \tag{5a,b}$$

(Surface tension effects are neglected.) Following (5a) we set $\xi(x,y) = \varphi(x,\eta(x,t),t)$ and define the Dirichlet-Neumann operator:

$$G(\eta)\xi = (1 + (\partial_x\eta)^2)^{1/2}\partial_n\varphi \quad \text{on } y = \eta, \tag{6}$$

where n is the exterior unit normal of the water surface. The operator $G(\eta)$ maps Dirichlet data to Neumann data on the free surface. It is linear in ξ but nonlinear, with explicit nonlocal dependence, on η which determines the fluid domain. In terms of the surface quantities η and ξ the free surface conditions of (5) become:

$$\partial_t \eta = G(\eta)\xi,$$
$$\partial_t \xi = -\frac{1}{2(1+(\partial_x \eta)^2)}\left((\partial_x \xi)^2 - (G(\eta)\xi)^2 - 2(\partial_x \eta)(\partial_x \xi)G(\eta)\xi\right) - g\eta. \quad (7a,b)$$

These are Hamilton's canonical equations in Zakharov's (1968) formulation of the water-wave problem as a Hamiltonian system, i.e.,

$$\partial_t \eta = \partial_\xi H, \qquad \partial_t \xi = -\partial_\eta H, \quad (8a,b)$$

with the Hamiltonian:

$$H = \tfrac{1}{2}\int\left(\xi G(\eta)\xi + g\eta^2\right)dx. \quad (9)$$

Coifman & Meyer (1985) showed that when $\eta \in Lip(\Re)$ the Dirichlet-Neumann operator can be written as a convergent Taylor series:

$$G(\eta) = \sum_{j=0}^{\infty} G_j(\eta), \quad (10)$$

and Craig & Sulem (1993) showed that explicit expressions for the G_j can be computed using a recursion formula.

The above system of equations are solved numerically for specified initial data using periodic boundary conditions in the x-direction and a pseudo-spectral method for the spatial discretization. The Dirichlet-Neumann operator is approximated by a finite number, M, of terms in (10). In practice, it is not necessary to use large values of M due to the fast convergence of the series expansion for $G(\eta)$. The two variables η and ξ are expanded in truncated Fourier series with the same number of modes. Applications of Fourier multipliers are performed in spectral space, while nonlinear products are calculated in physical space at a discrete set of equally spaced points. All operations are performed using the FFTW routines.

Time integration is performed in Fourier space. The linear terms in (7) are solved exactly by an integrating factor technique. The nonlinear terms are integrated using a fourth-order Adams-Bashford/Moulton predictor-corrector scheme with constant time step. In the computations it was observed that spurious oscillations developed in the wave profile after some time of integration due to onset of an instability initiated by growth of numerical errors at high wave-numbers. To circumvent this difficulty we applied an ideal low-pass filter to η and ξ at each time step.

2.3 KdV Models

An asymptotic approximation of the Euler equations in the limit of weak dispersion and weak nonlinearity is the well-known Korteweg-de Vries equation:

$$\eta_t + c_o\eta_x + \frac{3c_o}{2h}\eta\eta_x + \frac{1}{6}h^2 c_o \eta_{xxx} = 0. \tag{11}$$

Equation (11) is for right-running waves only; a similar KdV equation applies to left-running waves. The solitary-wave solution of (11) is:

$$\eta(x,t) = a_o \sec h^2\left[\sqrt{\frac{3a_o}{4h^3}}(x-ct)\right], \tag{12}$$

in which the speed of the wave is:

$$c = c_o\left(1+\frac{a_o}{2h}\right). \tag{13}$$

Wayne & Wright (2004) have shown formally that, to the KdV order of weak nonlinearity and dispersion, left-running and right-running solitary waves interact *linearly* during their collision. Hence, we will use linear superposition as an approximate model of head-on collisions for comparison with the fully nonlinear, numerical solutions of the Euler equations.

In the case of collisions among N co-propagating solitary waves Hirota (1971) found an exact solution of (11) when the reference frame translates to the right with the speed c_o. For the case of a binary ($N = 2$) collision (also see Whitham, 1974) the solution is:

$$\eta(x,t) = -2h\left[\frac{\left(\beta_1^2\theta_1 + \beta_2^2\theta_2 + 2(\beta_2-\beta_1)^2\theta_1\theta_2\right) + \frac{(\beta_2-\beta_1)^2}{(\beta_2+\beta_1)^2}\left(\beta_1^2\theta_1\theta_2^2 + \beta_2^2\theta_1^2\theta_2\right)}{\left[1+\theta_1+\theta_2+\frac{(\beta_2-\beta_1)^2}{(\beta_2+\beta_1)}\theta_1\theta_2\right]^2}\right], \tag{14}$$

in which:

$$\beta_1 = \sqrt{\frac{2a_1}{h}}, \quad \beta_2 = -\sqrt{\frac{2a_2}{h}}, \tag{15a,b}$$

$$\theta_1(x,t) = e^{-\beta_1(x-x_1)/h+\beta_1^3 t\sqrt{\frac{6h}{g}}}, \quad \theta_2(x,t) = e^{-\beta_2(x-x_2)/h+\beta_2^3 t\sqrt{\frac{6h}{g}}}, \quad (16a,b)$$

and (a_1, a_2) are the amplitudes of the two individual solitary waves and (x_1, x_2) are arbitrary (initial) shifts in wave positions.

4. Head-on (counter-propagating) collision

Specific procedures for the experiments on counter-propagating binary collisions of solitary waves are the following. Since only one wave-maker was available, it was necessary to generate a first solitary wave (a_o=2.00cm) that propagated down the channel and reflected from the end-wall. Subsequently a second solitary wave (a_o=1.25cm) was generated that collided with the reflected wave near the center of the channel test section. The instrument carriage was fixed during each experiment so as to provide a spatial window of the collision in the interval. Data were collected for about 64s so that the two solitary waves reflect and collide multiple times. Results for the first collision are reported herein.

Once the raw data (voltages) are converted to wave amplitudes using the calibration results, correlations are performed between the pressure measurement of the first experiment and that of each of other 39 experiments. In this manner we obtain the necessary time shifts to obtain the maximum correlation values among the 40 experiments. Typically, these shifts are about 0.01s. Initially we used the entire 64 seconds of pressure data to shift the records. The resulting spatial profiles were wholly unsatisfactory, exhibiting a lack of smoothness that was clearly an artifact of the data reduction algorithm. Second, we computed correlations using only an interval of the pressure data containing the first solitary wave before its' reflection. The resulting time shifts yielded excellent results for right-running waves as shown in Figure 2. However, the results for the reflected, left-running wave were non-smooth. An example of these results is shown in Figure 3a, which shows the counter-propagating waves prior to collision. Note that the non-smooth, left-running wave (on the right in the figure) has a jump discontinuity at one location. Third, correlations were performed using an interval of the pressure data containing the reflected (left-running) solitary wave. These time shifts resulted in smooth left-running spatial profiles, but non-smooth, right-running waves as shown Figure 3b. We conclude that the reflection process (or, perhaps, propagation through the boundary-layer wake left by the incident wave) produces a small (about 0.05s) shift in the wave arrival times at our measurement sight. This small shift is *random*, i.e., it differs for each experiment. Hence, we are not able to resolve both the left-running and right-running waves with a single correlation procedure. The results presented below use correlations based on the reflected wave as in Figure 3b.

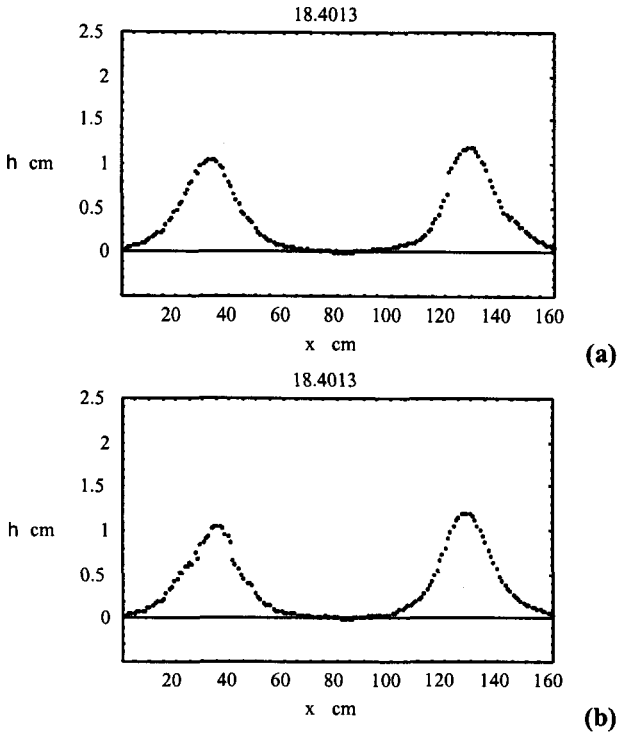

Figure 3. Counter-propagating solitary waves before collision (at t=18.4013s).
(a) Time shifts based on pressure data for first solitary wave before reflection.
(b) Time shifts based on pressure data for reflected solitary wave.

A sequence of spatial profiles during the collision of counter-propagating solitary waves is shown in Figure 4. The experimental times (in seconds) are shown above each profile. Note that the total collision interval spanned in Figure 4 is about 1.7s. The experimental data at t = 18.2999s were fit theoretically with the linear sum of two solitary waves having initial amplitudes of (right-running) and (left-running), respectively. This theoretical fit (dashed line) served as the initial data for the Euler computations. Recall that the experimental spatial profiles in Figure 4 are based on correlations that resolve the left-running wave best.

The spatial profiles of Figure 4 between the times of t = 18.7024s and t = 19.9205s for the left-running solitary wave agree well with both the linear superposition and Euler predictions, which are nearly the same. The maximum wave amplitude of the collision occurs in the spatial profile at t = 19.0311s

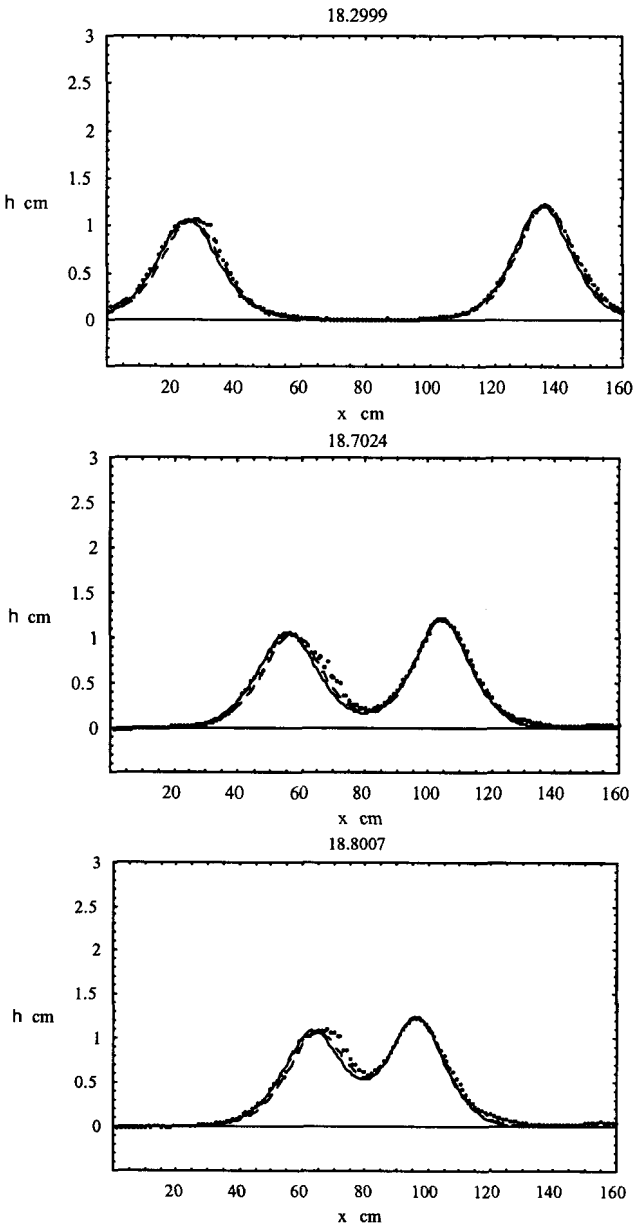

Figure 4. Spatial profiles of counter-propagating collision of two solitary waves at different times (listed above each frame). Solid points are experimental data. Solid line is Euler computations. Dashed line is linear superposition of KdV solitons.

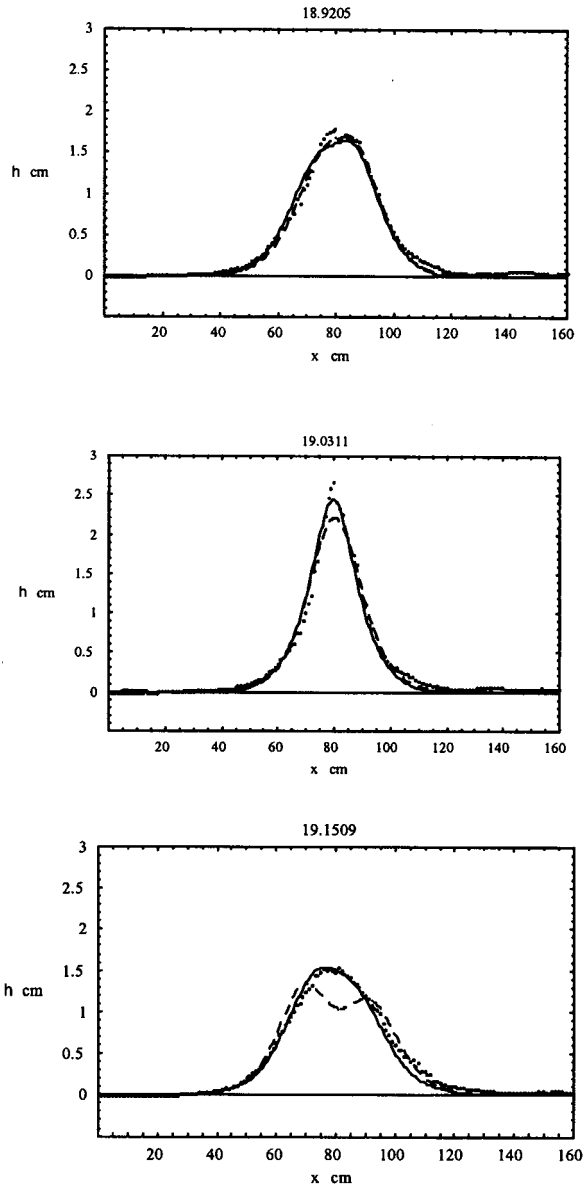

Figure 4. *Continued.*

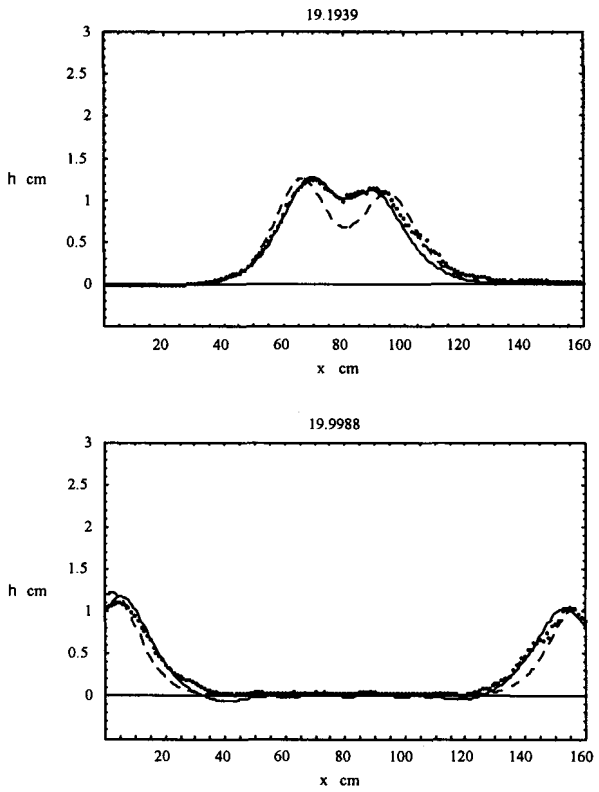

Figure 4. *Continued.*

according to both the measurements and the theories. Both the Euler prediction and the measured data (for the remnant of the left-running wave) agree, and the maximum amplitude is about 2.45cm -- linear superposition predicts 2.27cm. Subsequent to the time of maximum amplitude, the Euler predictions and the measured data agree well; however, there are now quite large discrepancies with linear superposition. In other words, linear superposition is fairly accurate until the maximum amplitude is achieved, but much less accurate thereafter. The last spatial profile at t = 19.0311s shows the two solitary waves after the collision. According to linear superposition there should be no phase shifts in consequence of the collision. Clearly both the experimental data and Euler computations show that a small phase shift has occurred, i.e., the collision has delayed both waves. The observed shift is increasing with propagation distance; hence, the collision was not elastic. Interestingly, Euler theory predicts slightly more phase shift than observed in the last frame.

5. Following (co-propagating) collision

Unlike the head-on collision described above, the collision of a larger solitary wave overtaking a smaller solitary wave occurs over a very large distance down the wave channel. In order to measure a following collision, the instrument carriage must move with the waves and measure in a traveling reference frame. The co-propagating collision experiments were conducted in the following manner. The instrument carriage was positioned near the wave-maker so that its' initial measurement window spanned. The wave-maker then generated a smaller solitary wave with a_o = 5cm followed immediately by a larger solitary wave with a_o = 2.00cm. Once these two waves reached the instrument-carriage window, the carriage accelerated smoothly for 2.5s and at a distance of 1.125m to a constant speed of 90 cm/s. The constant speed was maintained for 4.5s when the carriage decelerated for 2.5s and stopped. The total move time of motion for the carriage was 9.5s and the total move distance was 6.35m. Programmed and actual motions of the carriage are shown in Figure 5. It is important to note that the "actual" carriage displacement and velocity shown in Figure 5 is inferred from a rotary encoder on the back of the motor powering the belt drive attached to the carriage. This was necessary due to the long distance traversed by the carriage, which prohibited the use of a feedback sensor for the carriage position. Since the belt between the motor and the carriage is not rigid, there is necessarily uncertainty in carriage position, especially during the acceleration and deceleration intervals. Comparisons of carriage motions between two different experiments showed that the actual motion shown in Figure 5 is reproduced for each experiment.

Figure 6 shows the waves underneath the instrument-carriage window just before it begins moving. The dashed line is a 2-soliton solution (Equation 14) fit to the experimental data. The solid line, which agrees with the data much better, is the linear superposition of two solitary waves with $a_o = 2.15cm$ and $a_o = 0.68cm$. This linear fit is used as the initial data for the Euler computations. (It should be noted that the wave-maker motion corresponded to the linear superposition of two solitary waves also.)

A sequence of spatial profiles during the collision of two co-propagating solitary waves is shown in Figure 7. Times (in seconds) during the collision (measured from the initial data of Figure 6) are shown above each profile. At all times the Euler predictions agree with the measurements better than the KdV predictions. At all times the maximum amplitudes predicted by KdV model exceed those by the Euler model, which exceed those in the measurements. In addition, the discrepancies in maximum-amplitude predictions increase with time and distance down the channel. This behavior is consistent with viscous damping that is significant in these experiments in consequence of the long distances of propagation during the collision. The small differences in phases between the

predicted and measured positions of wave peaks, e.g. at $t = 8.79081$s, is due, in part, to viscous effects and, in part, to experimental errors in the resolution of carriage position.

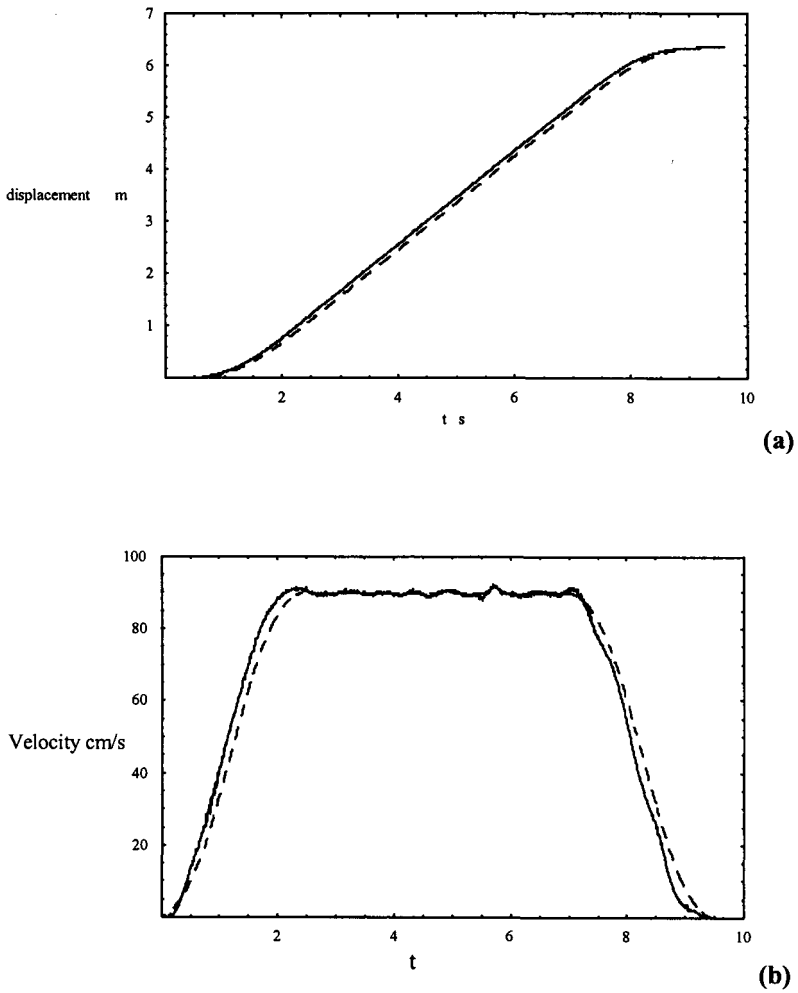

Figure 5. Actual (solid line) and programmed (dashed line) carriage motion. (a) Displacement, (b) Velocity.

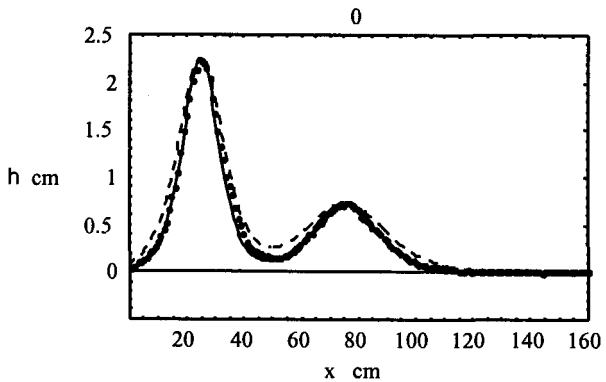

Figure 6. Initial data for co-propagating collision of two solitary waves. Solid points are data. Dashed line is a best fit of the 2-soliton solution. Solid line is best fit of a linear superposition of KdV solitons.

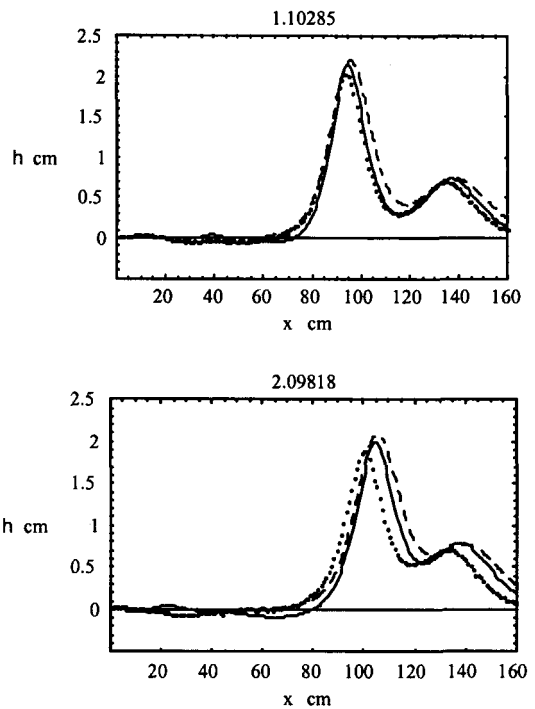

Figure 7. Spatial profiles of co-propagating collision of two solitary waves at different times (listed above each frame). Solid points are experimental data. Solid line is Euler computations. Figure Dashed line is 2-soliton solution of the KdV equation.

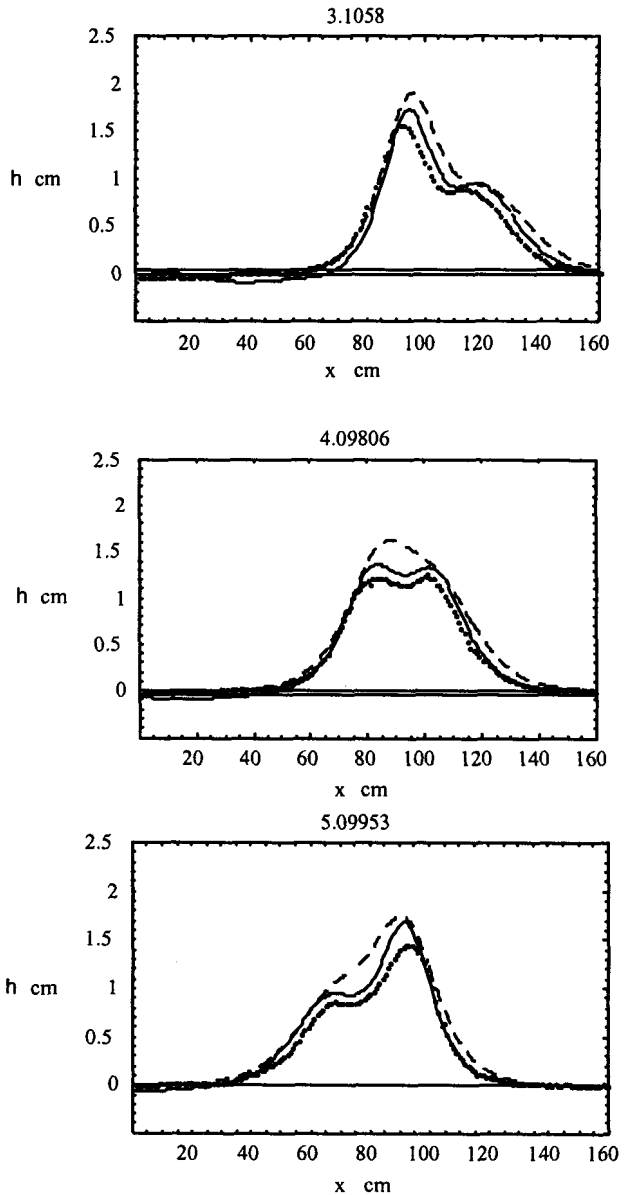

Figure 7. *Continued.*

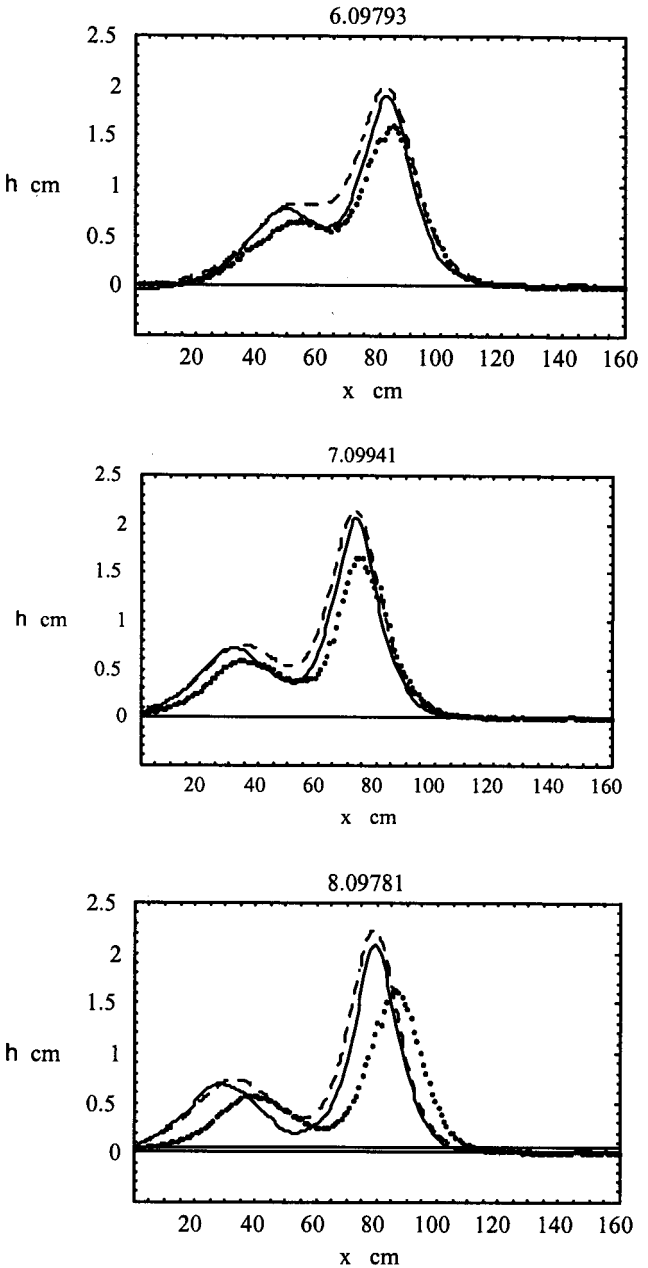

Figure 7. *Continued.*

As noted earlier, Wu (1998) shows that there is an instant in time during the collision of two co-propagating solitary waves for which the interaction profile exhibits fore-and-aft symmetry. This behavior is shown in Figure 7 by both the measured and Euler computations at $t = 4.09806$s. Interestingly, the KdV model does not show the fore-and-aft symmetry at this time.

6. Summary

High-resolution experimental data were presented for both co- and counter-propagating collisions between two solitary waves. The data are in the form of spatial wave profiles at fixed times during the collision. The data for the counter-propagating (head-on) collision are compared to numerical solutions of Euler equations and to linear superposition of two KdV solitary waves. Linear superposition is fairly accurate until the time at which maximum runup amplitude occurs. It is much less accurate thereafter. The Euler model predicts accurately the measured profiles and the resulting maximum runup amplitude and subsequent phase shifts. The maximum measured runup amplitude is 2.45cm, which is predicted by the Euler model. Linear superposition predicts a value of 2.27cm.

The Euler model also agrees well with the measured data for the following collision; however, it over-predicts wave amplitudes. This disagreement is anticipated since viscous damping over the long distance spanned by the collision is significant in the experiments. Both the experiments and the Euler model exhibit a profile with fore-and-aft symmetry as predicted by Wu (1998) at an instant during the collision. The 2-soliton solution of the KdV equation agrees qualitatively with the measurements. However, it greatly over predicts amplitudes (more than the Euler model), and it does not show a profile with fore-and-aft symmetry at the instant measured and predicted by the Euler equations.

References

Byatt-Smith, J.G.B. 1971. An integral equation for unsteady surface waves and a comment on the Boussinesq equation. *J. Fluid Mech.* 49, 625-633.

Byatt-Smith, J.G.B. 1989. The interaction of two solitary waves of unequal amplitude. *J. Fluid Mech.* 205, 573-579.

Coifman, R. & Y. Meyer 1985. Nonlinear harmonic analysis and analytic dependence, Pseudodifferential operators and Applications, Notre Dame IN (1984), Amer. Math. Soc., 71-78.

Craig, W. & C. Sulem 1993. Numerical simulation of gravity waves. *J. Comput. Phys.* 108, 73-83.

Gardner, C.S, J.M Greene, M.D.Kruskal, & R.M. Miura 1967. Method for solving the Korteweg-deVries eqation. *Phys. Rev. Lett.* 19, 1095-1097.

Goring, D.G. & F. Raichlen 1980. The generation of long waves in the laboratory. *Proc. 17th Intl Conf. Coastal Engrs*, Sydney, Australia.

Hirota, R. 1971. Exact solutions of the Korteweg-deVries equation for multiple collisions of solitons. *Phys. Rev. Lett.* 27, 1192-1194.

Korteweg, D.J. & G. deVries 1895. On the change of form of long waves advancing in a rectangular channel, and a new type of long stationary waves. *Phil. Mag. (5)* 39, 422-443.

Maxworthy, T. 1976. Experiments on the collisions between solitary waves. *J. Fluid Mech.* 76, 177-185.

Mayer, R.E. 1962. *Brown University Tech. Rept.*

Mirie, R.M. & C.H. Su 1982. Collisions between two solitary waves. Part 2. A numerical study. *J. Fluid Mech.* 115, 476-492.

Russell, J.S. 1845. Report on waves. *Brit. Assoc. Rept.*

Su, C.S. & R.M. Mirie 1980. On collisions between two solitary waves. *J. Fluid Mech.* 98, 509-525.

Wayne, C.E. & J.D. Wright 2004. Higher-order modulation equations for a Boussinesq equation. Preprint.

Weidman, P.D. & T. Maxworthy 1978. Experiments on strong interactions between solitary waves. *J. Fluid Mech.* 85,417-431.

Whitham, G.B. 1974. Linear and Nonlinear Waves. John Wiley & Sons.

Wu, Theodore Yaotsu 1998. Nonlinear waves and solitons in water. *Physica* D 123, 48-63.

Yih, C.S. & T.Y. Wu 1995. General solution for interaction of solitary waves including head-on collisions. *Acta Mech. Sinica* 11, 193-199.

Zabusky, N.J. & M.D. Kruskal 1965. Interactions of solitons in a collisionless plasma and the recurrence of initial states. *Phys. Rev. Lett.* 15, 240-243.

Zakharov, V.E. 1968. Stability of periodic waves of finite amplitude on the surface of a deep fluid. *J. Appl. Mech. Tech. Phys.* 9, 190-194.